Determination of the Effective Elastic Coefficients for Heterogeneous Media – 15109

Cheo Kyung Lee and Borey Long
Handong Global University
3 Namsong-ri, Heunghae-eub, Buk-gu, Pohang, Kyungbuk, 791-708
Republic of Korea

ABSTRACT

The effective elastic coefficients on the macroscale for heterogeneous media are calculated by solving the micro-cell elastostatic problem numerically. The cell problem is obtained by applying the homogenization theory to periodic composite media. Two different types of inclusion geometry are considered: (i) a circle and (ii) a circle with longitudinal ribs of small rectangular cross-section. The deformation is caused by traction force distributed along the interface between the two regions of different elastic moduli. The displacements are calculated by using ABAQUS and are used to determine the effective elastic coefficients on the macroscale. It is shown that the elastic coefficients are larger for (ii) than (i) due to the ribs thereby enhancing the elastic rigidity.

INTRODUCTION

The strength of structures is usually enhanced by inserted components of higher strength. Concrete structures are always enhanced by steel reinforcement bars embedded in the region where tensile force is applied. For safe operation of underground nuclear waste repository it is important to secure large enough elastic properties for reliable functioning of the facility. Therefore it is essential to know the elastic characteristics of composite media which in general have inclusions of higher rigidity.

In this study, micro-cell geometries with inclusions of the shape (i) circular cross-section, and (ii) circular cross-section with ribs at the top and bottom of the cross-section are considered: It is assumed that these inclusions are distributed periodically in space in the solid background medium.

The theoretical approach is based on the homogenization theory which systematically combines the processes on the microscale(of order ℓ) and deduces the governing equations and the effective coefficients on the macroscale(of order L) [1]. It is assumed that the two spatial scales are disparate so that $\ell << L$. Under two basic assumptions, (i) the periodicity of the medium structure on the microscale with periodic length l and (ii) the periodicity of all variables and material properties with the same periodic length l. The periodicity assumption is not restrictive because the distributions and arrangements over the periodic length are quite arbitrary and pretty much all conceivable distribution patterns are possible. Only the efforts to carry out the elastostatic analysis will be different depending on the complexity of the distribution inside the unit micro-cell.

The theoretical developments start from the basic governing laws on the microscale (the equilibrium equations and constitutive laws). With multiple-scale perturbation expansion the governing laws on the macroscale are deduced with no recourse to empirical or experimental assumptions. Throughout the process certain microscale boundary-value problems in a unit cell are defined whose solutions are used in the calculation of the effective macroscale elastic coefficients. If the inclusion geometry is specified, the solution to the unit cell problem is found by numerical method. The software package ABAQUS is specifically used to carry out solving the elastostatic boundary-value problems defined on the microscale.

It is shown that the effective macroscale elastic coefficients increase with the increase of the volumetric portion of the stronger phase. Also the increase of the elastic coefficients is larger for transverse ones than the longitudinal ones for inclusion geometry with ribs attached to it due to the latching effect of the ribs.

It is noted that the computational approach adopted in this study starts from the basic governing relations on the microscale without making empirical or phenomenological assumptions. Then the multiple-scale analysis is used to deduce the effective relations (governing equations and constitutive laws) on the microscale.

THE GOVERNING RELATIONS ON THE MICROSCALE

The composite medium is assumed to be composed of a solid region($\Omega 1$) and another solid region($\Omega 2$) that fill the unit cell on the microscale. Each region is assumed to be connected throughout the composite medium. Solid deformation takes palce by macroscopically imposed strain over the medium.

The basic governing equations in the solid domains ($\Omega 1$ and $\Omega 2$) and the boundary conditions on the interface(Γ) are described which is given in the process of multiple-scale expansion.
In each region, the quasi-static equilibrium equation with Hooke's law must be satisfied.

On the boundary Γ between the two regions, the continuity of the displacement, and the continuity of stress must be satisfied.
In summary, the equilibrium equation and the Hooke's law are written as

$$\nabla \cdot {}^{[a]}\boldsymbol{\sigma} = \frac{\partial\, {}^{[a]}\sigma_{ij}(\mathbf{x})}{\partial x_j} = 0 \qquad \mathbf{x} \in \Omega_a \ (a = 1, 2) \tag{Eq. 1}$$

$${}^{[a]}\sigma_{ij} = C^{[a]}_{ijkl}\, {}^{[a]}e_{kl} \quad \mathbf{x} \in \Omega_a \ (a = 1, 2) \tag{Eq. 2}$$

where ${}^{[a]}\sigma_{ij}$ and ${}^{[a]}e_{kl}$ are the solid stress and strain in Ω_a and $C^{[a]}_{ijkl}$ is the elastic coefficient tensor of rank 4. Summation is assumed for repeated indices (summation convention). The number in the brackets in left upper corner denotes the regions.

The boundary conditions on Γ are

$${}^{[1]}v_i = {}^{[2]}v_i \quad \mathbf{x} \in \Gamma \tag{Eq. 3}$$

$${}^{[1]}\sigma_{ij} n_j = {}^{[2]}\sigma_{ij} n_j \quad \mathbf{x} \in \Gamma \tag{Eq. 4}$$

where n_j is the unit normal vector on Γ pointing from $\Omega 1$ to $\Omega 2$.
The governing equations and the boundary conditions are then normalized and the multiple-scale expansion is carried out.

MULTIPLE SCALE ANALYSIS

Recognizing the scale disparity in the process of elastic deformation, two distinct length scales are introduced: the microscale length (the fast scale which is equivalent to the representative elementary volume in the traditional treatment of the process) and the macroscale length (the scale over which the processes of interest take place from the viewpoint of reservoir engineering and management).

The variables are expanded as perturbation series in the following small parameter

$$\frac{\ell}{L} = \epsilon << 1 \qquad \text{(Eq. 5)}$$

in which ℓ is the microscale length and ℓ' is the macroscale length. Upon expansion of the governing equations and boundary conditions, the microscale boundary-value problems are investigated according to the respective order of ϵ and the effective macroscale governing equations and coefficients are derived.

In the process of the multiple scale analysis, two canonical micro-cell boundary-value problems are defined whose solutions are used in the calculation of the effective medium properties(effective macroscale coefficients) by averaging over the micro-cell volume[2].

THE MICRO-CELL BOUNDARY-VALUE PROBLEMS

If the solid displaement is expanded in a perturbation series,

$$^{[a]}\mathbf{v} = {}^{[a]}\mathbf{v}^{(0)} + \epsilon\ {}^{[a]}\mathbf{v}^{(1)} + \epsilon^2\ {}^{[a]}\mathbf{v}^{(2)} + \cdots \qquad \mathbf{x} \in \Omega_a\ (a = 1, 2) \qquad \text{(Eq. 6)}$$

the leading order term $^{[a]}\mathbf{v}^{(0)}$ is independent of the microscale and the correction terms are expressed as

$$^{[a]}\mathbf{v}^{(1)} = {}^{[a]}\boldsymbol{\phi} : e'(\mathbf{v}^{(0)}) + \left\langle {}^{[a]}\mathbf{v}^{(1)} \right\rangle = {}^{[a]}\phi_i^{mn} e'_{mn}(\mathbf{v}^{(0)}) + \left\langle {}^{[a]}v_i^{(1)} \right\rangle \qquad \mathbf{x} \in \Omega_a\ (a = 1, 2) \qquad \text{(Eq. 7)}$$

where $\left\langle {}^{[a]}v_i^{(1)} \right\rangle$ is the unit-cell average of the left-hand side. The unit-cell average is defined as

$$\langle f \rangle = \frac{1}{\Omega} \int_{\Omega} d\Omega \qquad \text{(Eq. 8)}$$

The unknown functions $^{[a]}\boldsymbol{\phi} = {}^{[a]}\phi_i^{mn}\ (a = 1, 2)$ are the displacements in *i*-th direction due to macroscale unit strain $e'_{mn}(\mathbf{v}^{(0)})$ in Ω_a. They are the solutions of the following boundary-value problems:

$$\nabla \cdot [\mathbf{C}^{[1]} : \mathbf{e}({}^{[1]}\boldsymbol{\phi})] + (\nabla \cdot \mathbf{C}^{[1]}) : \mathbf{II} = 0 \quad \mathbf{x} \in \Omega_1 \qquad \text{(Eq. 9a)}$$

$$\nabla \cdot [\mathbf{C}^{[2]} : \mathbf{e}({}^{[2]}\boldsymbol{\phi})] + (\nabla \cdot \mathbf{C}^{[2]}) : \mathbf{II} = 0 \quad \mathbf{x} \in \Omega_2 \qquad \text{(Eq. 9b)}$$

$${}^{[1]}\boldsymbol{\phi} = {}^{[2]}\boldsymbol{\phi} \quad \mathbf{x} \in \Gamma \qquad \text{(Eq. 9c)}$$

$$\mathbf{C}^{[1]} : [\mathbf{II} + \mathbf{e}({}^{[1]}\boldsymbol{\phi})] \cdot \mathbf{n} = \mathbf{C}^{[2]} : [\mathbf{II} + \mathbf{e}({}^{[2]}\boldsymbol{\phi})] \cdot \mathbf{n} \quad \mathbf{x} \in \Gamma \qquad \text{(Eq. 9d)}$$

$$< {}^{[1]}\boldsymbol{\phi} > = < {}^{[2]}\boldsymbol{\phi} > = 0 \qquad \text{(Eq. 9e)}$$

Equations (Eq. 9a) and (Eq. 9b) are the equilibrium equations in Ω_1 and Ω_2. Equations (Eq. 9c) and (Eq. 9d) are the continuity relations for the displacement and the traction on the interface. Equations (Eq. 9e) is imposed for the uniqueness of the solutions.

The effective elastic coefficients on the macrosclae are given as

$$C'_{ijab} = \left\langle C^{[1]}_{ijab} \right\rangle + \left\langle {}^{[1]}\sigma_{ij}({}^{[1]}\boldsymbol{\phi}^{ab}) \right\rangle + \left\langle C^{[2]}_{ijab} \right\rangle + \left\langle {}^{[2]}\sigma_{ij}({}^{[2]}\boldsymbol{\phi}^{ab}) \right\rangle \qquad \text{(Eq. 10)}$$

It is composed of two part : the volume weighted average of the elastic coefficients and the stress due to $^{[a]}\phi$.

THE MICROCELL GEOMETRY, COMPUTATIONAL DOMAIN, AND MESH

Two types of microcell geometry are considered as shown in Fig. 1 in which Ω_1 in the shape of circular cross-section (Fig. 1(a) and (b)) and Ω_1 in the shape of circular cross-section with small rectangular ribs at the top and bottom are shown in (c) and (d). The cell shown in Fig. 1(a) has dimensionless size of unity in both horizontal and vertical directions. The radius of the circular cross-section is chosen to be 0.1, 0.125 and 0.16.

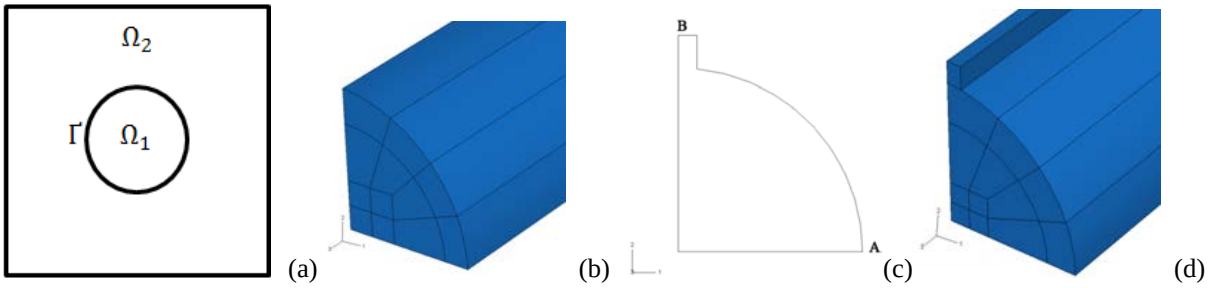

Fig.1. The microcell geometry: (a) Front view, (b) Ω_1 in the shape of circular cross-section, (c) Front view of circular cross-section with ribs, (d) Ω_1 in the shape of circular cross-section with small rectangular ribs at the top and bottom.

Due to the symmetry of the traction force distribution about the horizontal and vertical centerlines on Γ, the computaional domain is reduced to one quarter (the first quadrant) of Fig. 1(a). The computation has been carried out in the reduced domain by using elastic analysis part of ABAQUS with quadratic 3D finite elements so that there are 20 nodes in each element. The computational domain is the specified as $0<x<0.5$, $0<y<0.5$, $0<z<1.0$.

Three progressively finer meshes are shown in Fig. 2 for the case of inclusion with circular cross-section. Since the medium response is expected to vary sharply at and near the interface where the traction force is applied, much finer meshes were used in that region.

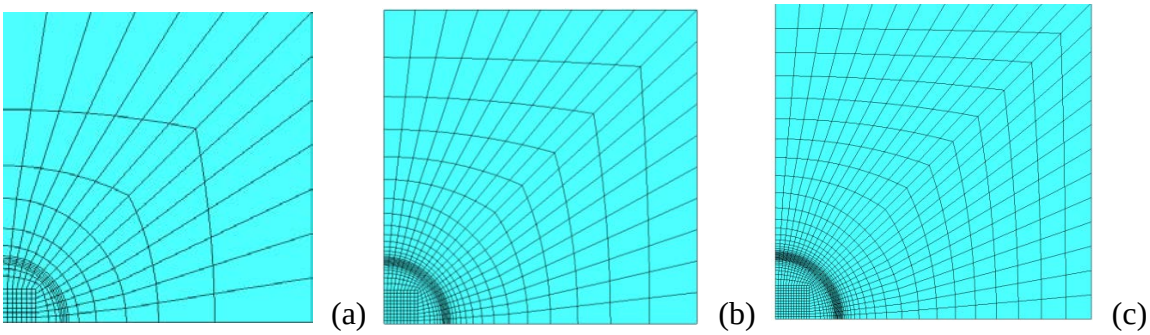

Fig. 2. Three different meshes: (a) Coarse, (b) Fine, and (c) Finer.

PROPERTIES OF THE SOLID MATERIALS IN Ω_1 AND Ω_2.

The solid materials in Ω_1 and Ω_2 are assumed to be isotropic. The elastic coefficient tensor is then[3]

$$C^{[a]}_{ijk\ell} = \lambda^{[a]}\delta_{ij}\delta_{k\ell} + \mu^{[a]}(\delta_{ik}\delta_{j\ell} + \delta_{i\ell}\delta_{jk}), \quad \lambda^{[a]} = \frac{E^{[a]}\nu^{[a]}}{(1-\nu^{[a]})(1-2\nu^{[a]})}, \quad \mu^{[a]} = \frac{E^{[a]}}{2(1+2\nu^{[a]})}$$

$$(a = 1, 2) \qquad \text{(Eq. 11)}$$

where $\lambda^{[a]}$ and $\mu^{[a]}$ are the Lame constants in Ω_a and δ_{ij} is the Kronecker delta. They are normalized by $E^{[1]}$ as follows:

$$\lambda^{[1]*} = \frac{\lambda^{[1]}}{E^{[1]}}, \ \lambda^{[2]*} = \frac{\lambda^{[2]}}{E^{[1]}}, \ \mu^{[1]*} = \frac{\mu^{[1]}}{E^{[1]}}, \ \mu^{[2]*} = \frac{\mu^{[2]}}{E^{[1]}} \qquad \text{(Eq. 12)}$$

in which symbols with overhead symbol * are dimensionless.

The physical values are chosen as follows:

$E^{[1]}$ =2x10^{11} Pa, $\nu^{[1]}$=0.8; $E^{[2]}$=2x10^{10} Pa, $\nu^{[2]}$=0.21 (Eq. 13)

They are typical of steel and concrete. Hence the micro-cell can be regarded as realization of concrete material enhanced by steel bars either without or with ribs. The normalized elastic coefficients then become

$$C^{[1]}_{xxxx}{}^{*} = \lambda^{[1]*} + 2\mu^{[1]*} = 1.3461, \quad C^{[1]}_{xxyy}{}^{*} = \lambda^{[1]*} = 0.5769, \quad C^{[1]}_{xyxy}{}^{*} = 2\mu^{[1]*} = 0.7692$$

$$C^{[2]}_{xxxx}{}^{*} = \lambda^{[2]*} + 2\mu^{[2]*} = 0.11251, \quad C^{[2]}_{xxyy}{}^{*} = \lambda^{[2]*} = 0.0299, \quad C^{[2]}_{xyxy}{}^{*} = 2\mu^{[2]*} = 0.0826 \qquad \text{(Eq. 14)}$$

$$C^{[a]}_{xxxx}{}^{*} = C^{[a]}_{yyyy}{}^{*} = C^{[a]}_{zzzz}{}^{*} \quad C^{[a]}_{xxyy}{}^{*} = C^{[a]}_{yyzz}{}^{*} = C^{[a]}_{zzxx}{}^{*} \quad C^{[a]}_{xyxy}{}^{*} = C^{[a]}_{yzyz}{}^{*} = C^{[a]}_{zxzx}{}^{*} \ (a = 1, 2)$$

NUMERICAL RESULTS AND DISCUSSION

In this study, the case *ab=xx* in (Eq. 10) only is discussed, i.e., the macroscale strain is a normal one in the x-direction. The numerical results obtained from the finest mesh are shown.

(1) Circular Inclusion

The displacements ϕ^{xx}_x and ϕ^{xx}_y are shown in Fig. 3 (a) and (b). The strains $e_{xx}(\boldsymbol{\phi}^{xx})$, $e_{yy}(\boldsymbol{\phi}^{xx})$ and $e_{xy}(\boldsymbol{\phi}^{xx})$ are shown in Fig. 4 (a) - (c). Also the stresses $\sigma_{xx}(\boldsymbol{\phi}^{xx})$, $\sigma_{yy}(\boldsymbol{\phi}^{xx})$, and $\sigma_{xy}(\boldsymbol{\phi}^{xx})$ are shown in Fig. 5 (a) - (c). In each of the plots, for detailed display of the variables, the two regions are enlarged nea the interface and are shown separately.

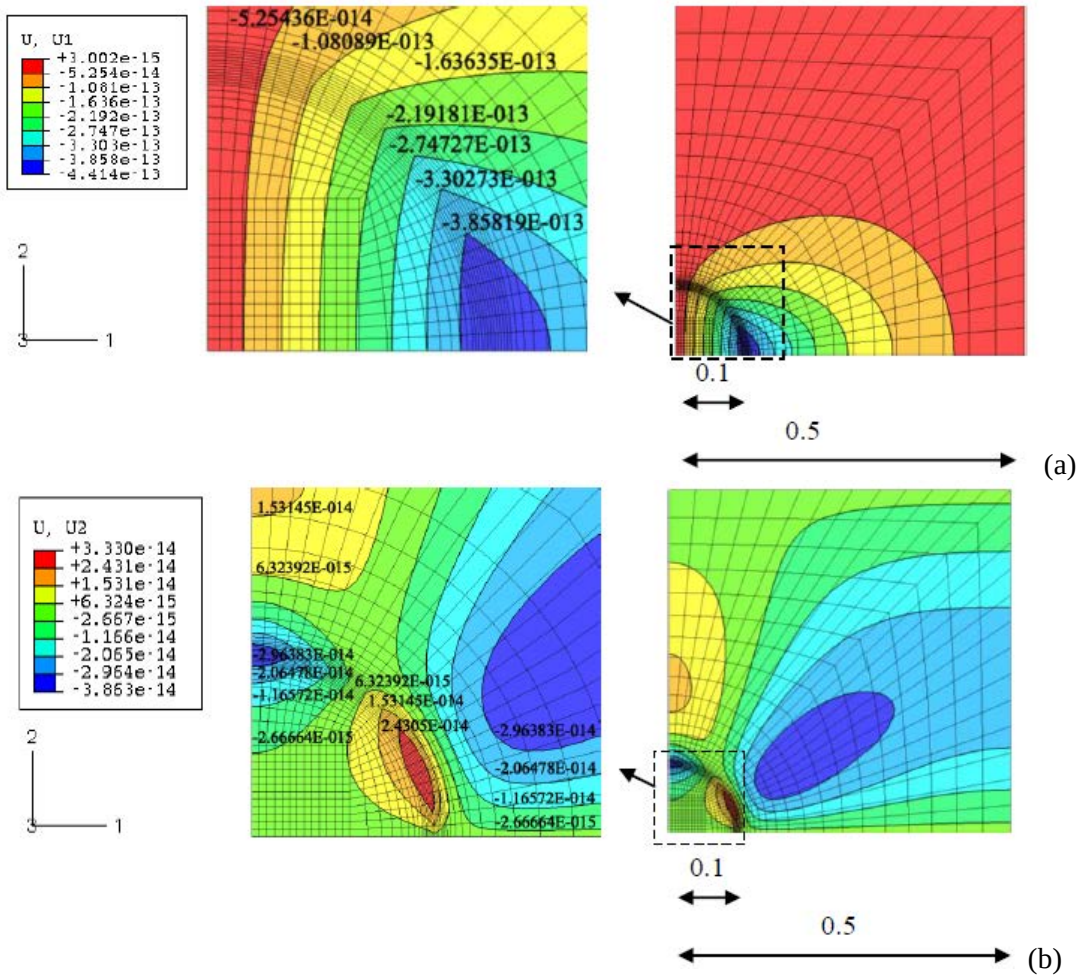

Fig. 3. The displacements (a) ϕ_x^{xx} and (b) ϕ_y^{xx}.

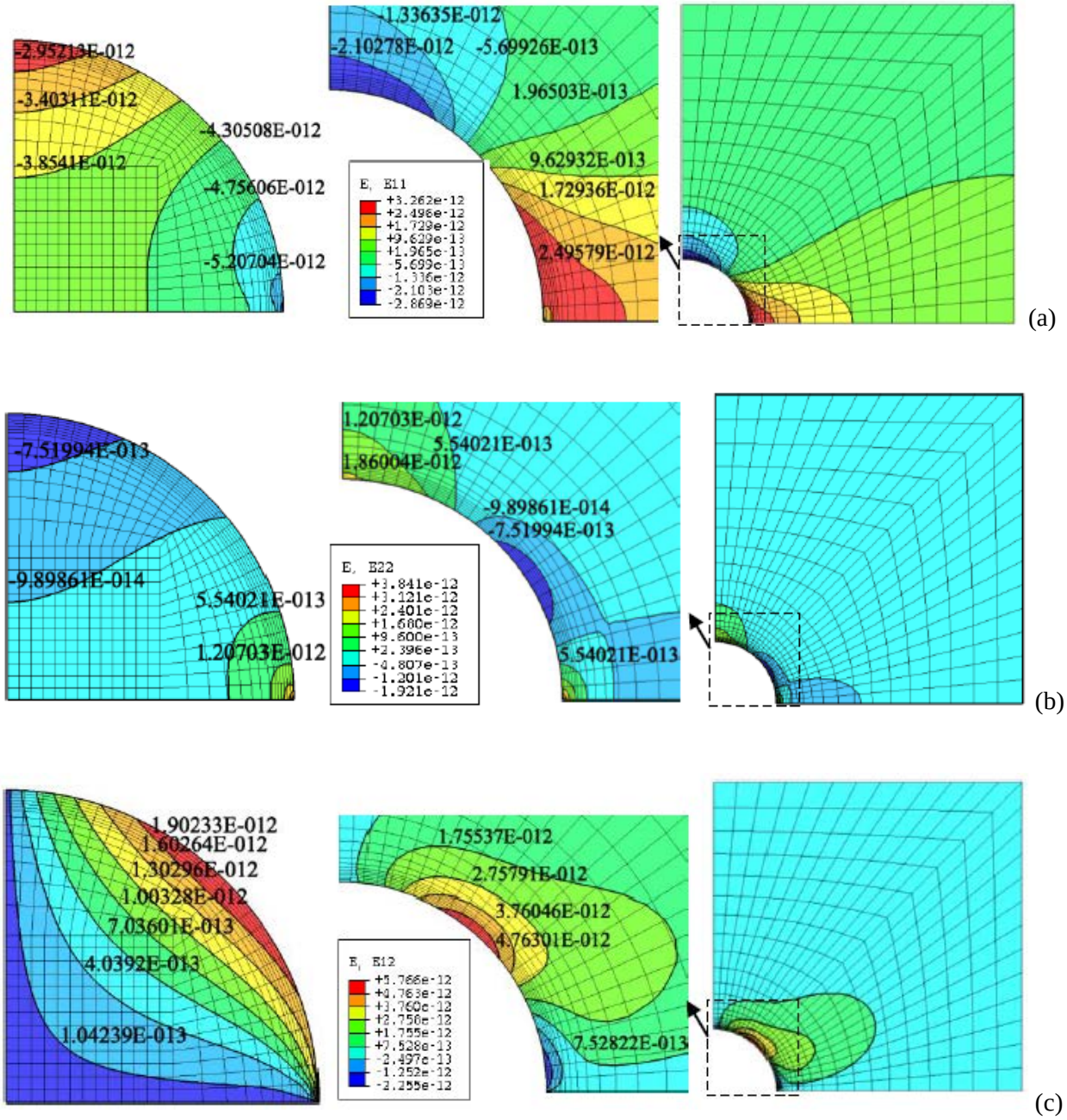

Fig. 4. The strains (a) $e_{xx}(\boldsymbol{\phi}^{xx})$, (b) $e_{yy}(\boldsymbol{\phi}^{xx})$, and (c) $e_{xy}(\boldsymbol{\phi}^{xx})$.

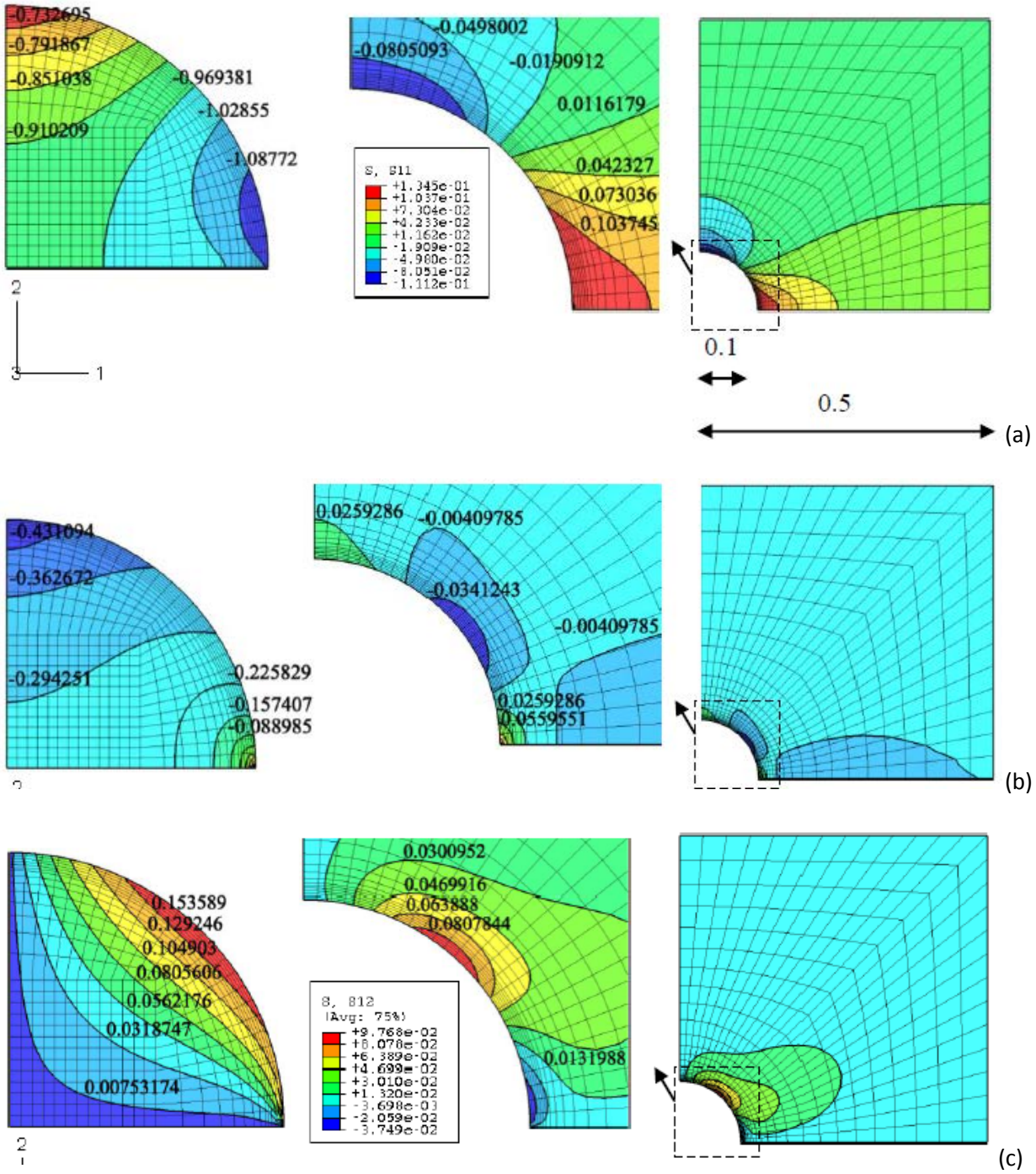

Fig. 5. The stresses (a) $\sigma_{xx}(\phi^{xx})$, (b) $\sigma_{yy}(\phi^{xx})$, and (c) $\sigma_{xy}(\phi^{xx})$.

(2) Circular Inclusion With Ribs

As in the case without ribs, the displacements ϕ_x^{xx} and ϕ_y^{xx} are shown in Fig. 6 (a) and (b). The strains $e_{xx}(\boldsymbol{\phi}^{xx})$, $e_{yy}(\boldsymbol{\phi}^{xx})$ and $e_{xy}(\boldsymbol{\phi}^{xx})$ are shown in Fig. 7 (a) - (c). Also the stresses $\sigma_{xx}(\boldsymbol{\phi}^{xx})$, $\sigma_{yy}(\boldsymbol{\phi}^{xx})$, and $\sigma_{xy}(\boldsymbol{\phi}^{xx})$ are shown in Fig. 8 (a) - (c).

(a)

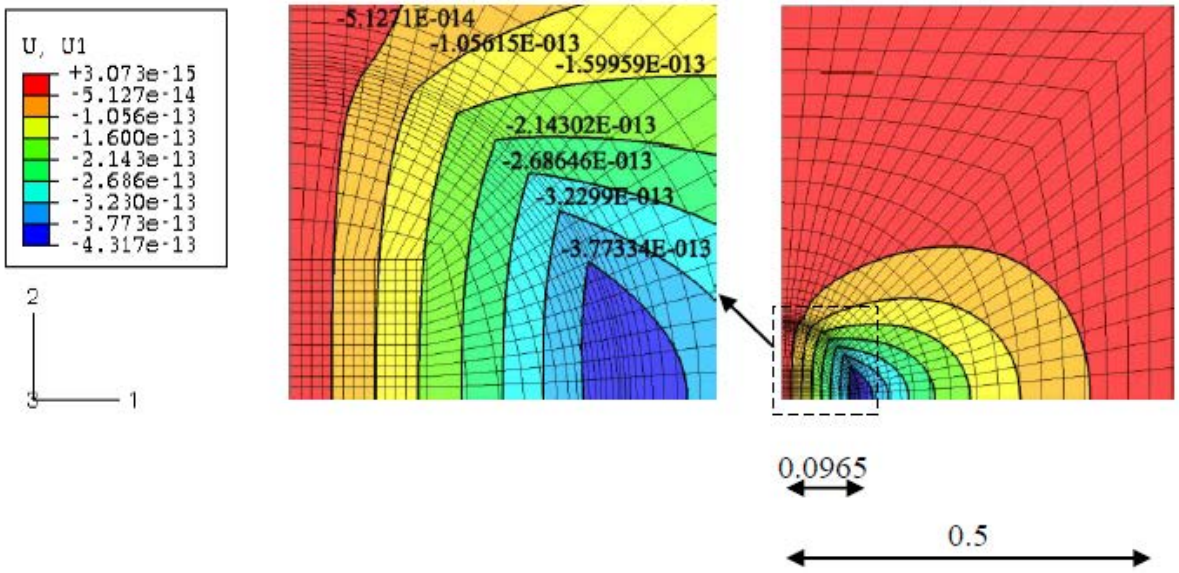

(b)

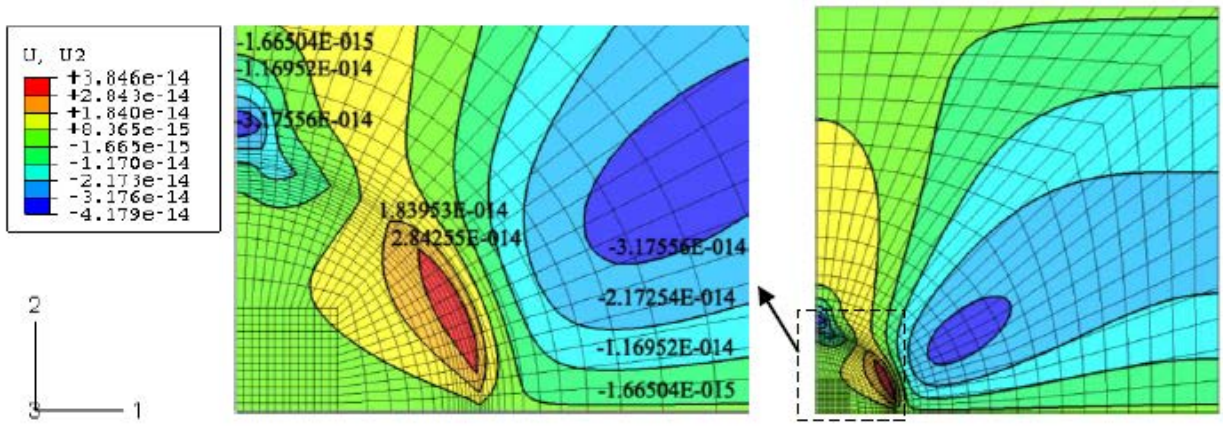

Fig. 6. The displacements (a) ϕ_x^{xx} and (b) ϕ_y^{xx} for circular bar with ribs..

(a)

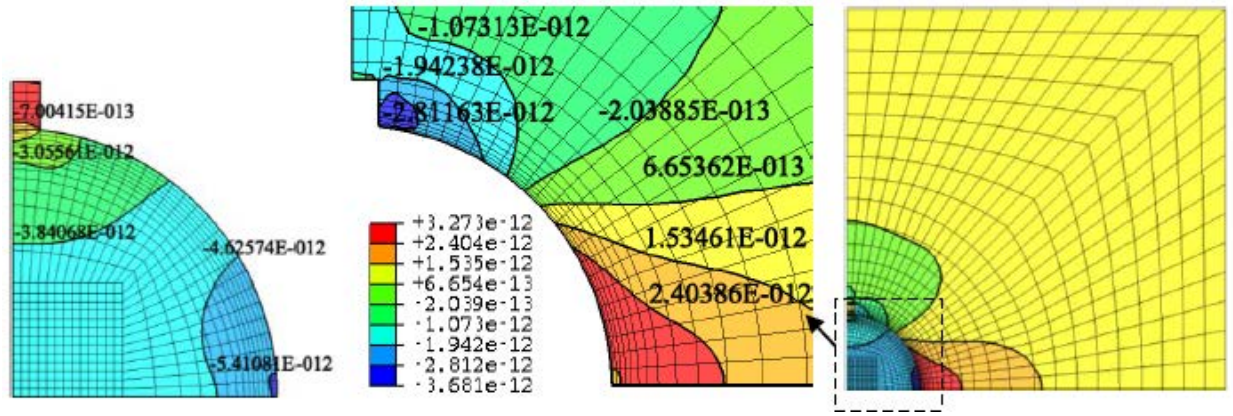

(b)

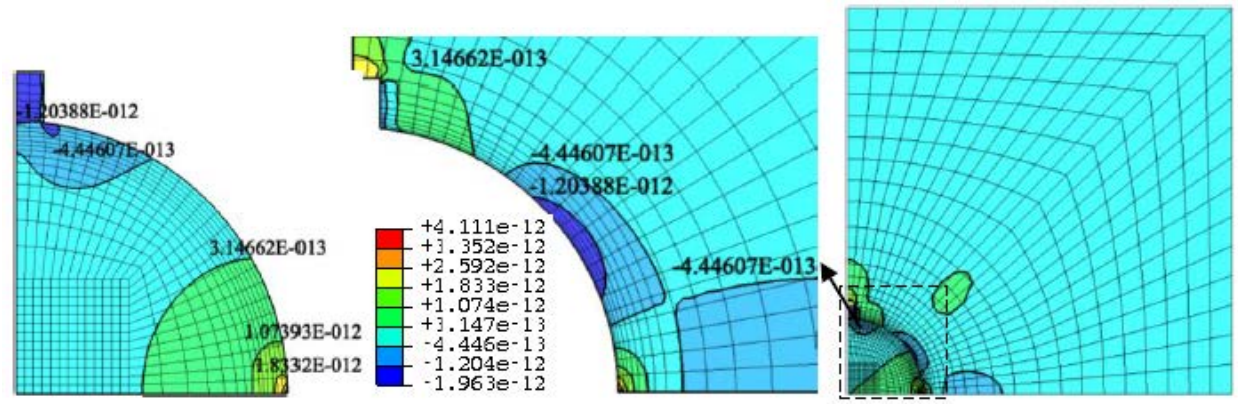

(c)

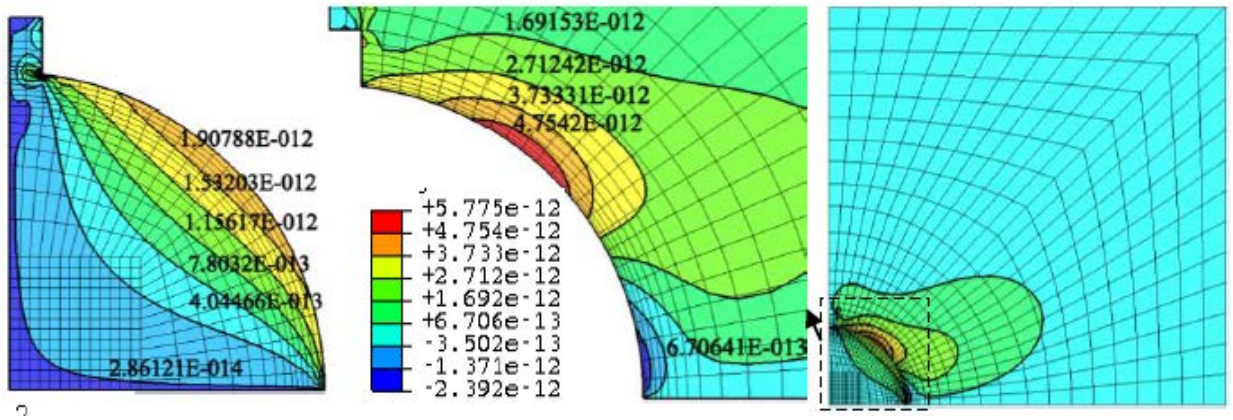

Fig. 7. The strains (a) $e_{xx}(\boldsymbol{\phi}^{xx})$, (b) $e_{yy}(\boldsymbol{\phi}^{xx})$, and (c) $e_{xy}(\boldsymbol{\phi}^{xx})$ for circular bar with ribs.

(a)

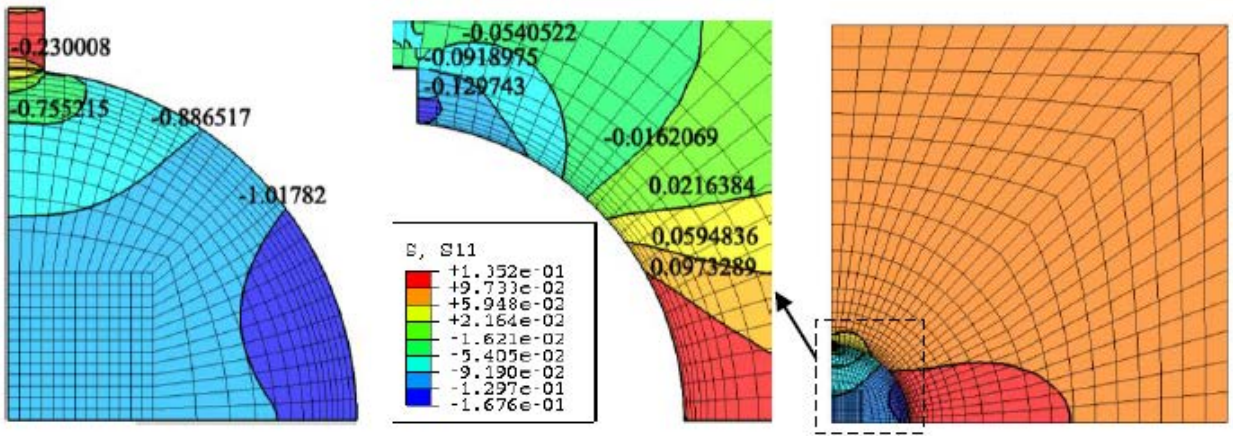

(b)

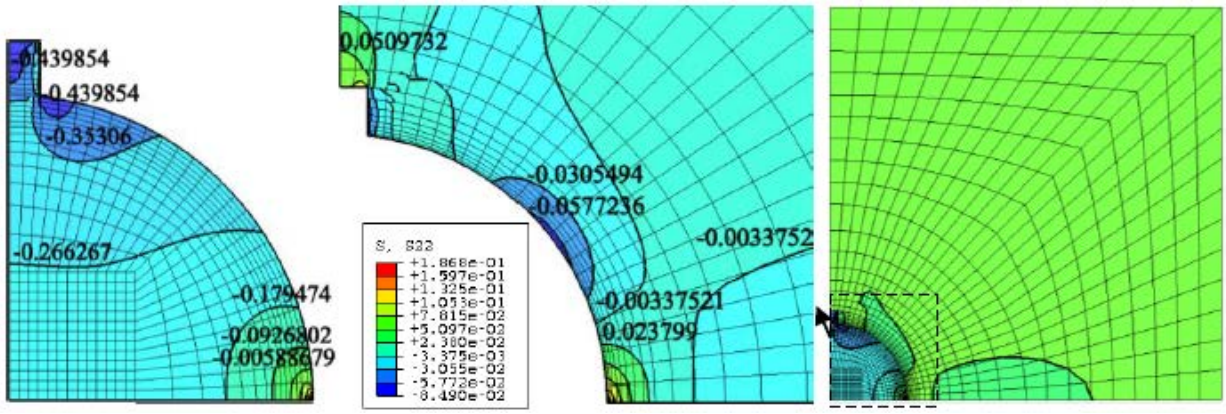

(c)

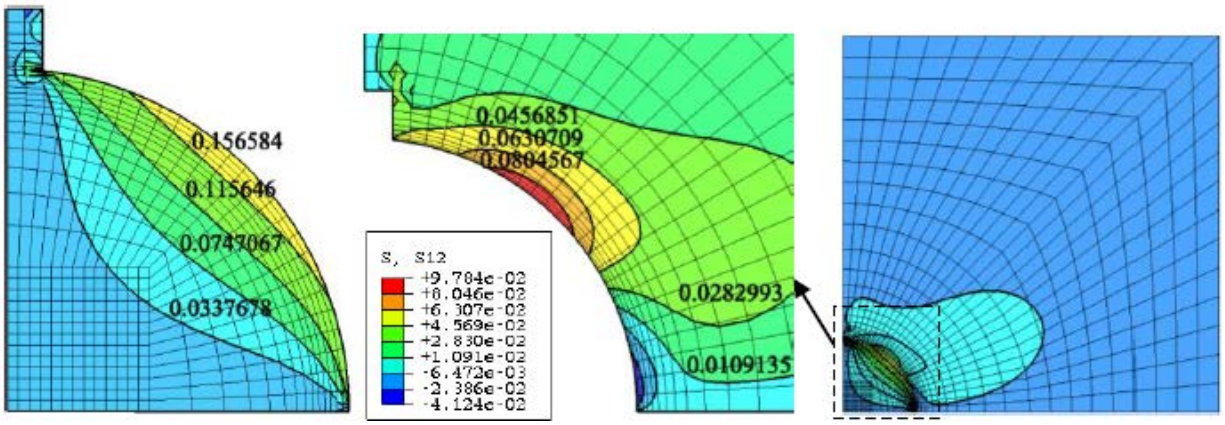

Fig. 8. The stresses (a) $\sigma_{xx}(\phi^{xx})$, (b) $\sigma_{yy}(\phi^{xx})$, and (c) $\sigma_{xy}(\phi^{xx})$ for circular bar with ribs.

NUMERICAL RESULTS AND DISCUSSION ON ELASTIC COEFFICIENTS

From the calculations with the finest meshes in the previous section and (Eq. 11), the effective elastic coefficients on the macroscale are summarized in Table 1 for circular inclusion and in Table 2 for circular inclusion with ribs. In the tables, *R* is the radius of the inclusion, and f_1 and f_2 are the volume fractions of each region.

(1) Circular Inclusion

Table 1. The effective elastic coefficients for circular inclusion

R	f_1	f_2	C'_{xxxx}	$C'_{yyxx} = C'_{zzxx}$
0.1	0.0314	0.9686	0.1673	0.0451
0.125	0.0491	0.9509	0.2301	0.0577
0.16	0.0804	0.9196	0.2707	0.0789

As the size of Ω_1 increases, i.e., as *R* increases, the longitudinal and transverse elastic coefficients increase. This is due to the contrast of *E* in Ω_1 and Ω_2. Recall from (Eq. 13) that $E^{[1]}$=2x10^{11} Pa and $E^{[2]}$=2x10^{10} Pa. Therefore if *R* increases, the elastic modulus increases.

(2) Circular Inclusion With Ribs

Table 2. The effective elastic coefficients for circular inclusion with ribs

R	f_1	f_2	C'_{xxxx}	$C'_{yyxx} = C'_{zzxx}$
0.1	0.0299	0.9701	0.1789	0.0523
0.125	0.0471	0.9529	0.2522	0.0644
0.16	0.0769	0.9231	0.2968	0.0921

In this case, the radius of the inclusion along the y-direction, that is the rib is included in measuring the radius. Hence the area of Ω_1 is a little bit reduced whreas as , the area of Ω_2 is increased by the same amount as compared with Case (1) above.

The elastic coefficients also increase as *R* increases in both longitudinal and transverse ones. It is noted that the increases is more pronounced for the transverse one than the longitudinal one.

CONCLUSIONS

From the calculations of the effective elastic coefficients for a composite material with inclusions of a circular shape and another circular shape with ribs the following conclusions are drawn.

1. The elastic coefficients increase with increasing volumetric portion of stronger phase which is intuitively obvious.
2. With ribs of quite small size attached to the surface of the inclusion, the elastic coefficients are increased thereby enhancing the composite material.
3. The rate of increase in the elastic coefficient for inclusions with ribs is larger for the transverse one than the longitudinal one. It is because of the latching effect of the ribs
4. Enhancement of composite materials with ribs can be effectively used in the design of underground nuclear waste storage facility for which utmost level of reliability and confidence are required.
5. It is worthwhile applying the computational approach adopted here to various other inclusion geometries and attachments to seek the optimal enhancement of structures.

|REFERENCES

1. C.K. LEE, "The Effective Elastic Coefficients of Porous Media with Simple Pore Geometries, Waste Management 14, Phoenix, AZ, USA.(2014).
2. C.K. LEE, M.Z. Htway, and S. P. YIM, "Permeability and Dispersion Coefficients in Rocks with Fracture Network", Waste Management 14, Phoenix, AZ, USA. .(2014).
3. Y.C. FUNG, *Foundations of Solid Mechanics*, Prentice-Hall (1965).

ACKNOWLEDGEMENT

This research was supported by the National Research Foundation of Korea (Grant: NRF-2012R1A1A2041369) funded by the Ministry of Education, Science and Technology. The financial support is gratefully acknowledged.